This article has been accepted for publication in a future issue of this journal, but has not been fully edited. Content may change prior to final publication. Citation information: DOI 10.1109/TPEL.2017.2773129, IEEE Transactions on Power Electronics

Dynamic Hysteresis Torque Band for Improving the Performance of Lookup-Table-Based DTC of Induction Machines

Ibrahim Mohd Alsofyani, *Member, IEEE,* Nik Rumzi Nik Idris, *Senior Member, IEEE* and Kyo-Beum Lee, *Senior Member, IEEE*

***Abstract*-- The magnitude of hysteresis torque band has a considerable effect on the performance of two-level Direct Torque Control (DTC) of induction machines. The conventional DTC fails at low speed due to the poor flux regulation. In this paper, two dynamic hysteresis torque band (DHTB) strategies for the conventional DTC are proposed to solve this problem by dynamically altering the amplitude of hysteresis torque band based on a flux error range. In this way, the simplicity of DTC algorithm is retained since it only requires a minor modification on its structure. The paper also presents further analysis on flux degradation, particularly the droop in between the flux sectors. In addition, the switching frequency effect of reverse voltage vectors for both DHTB schemes is investigated on the performance of the speed-sensorless DTC drive. The effectiveness of the proposed schemes is confirmed by simulation and experimental validation. Results show a significant enhancement in the flux regulation and dynamic torque response from zero motor speed.**

***Index Terms*-- Dynamic hysteresis torque band; direct torque control, flux regulation, induction motor, sensoless control.**

I. Introduction

THE interest in the research on direct torque control (DTC) of induction motors (IMs) has dramatically increased in the past decades due to the growing demand of high performance and high efficient drives for industrial applications. Excellent torque response, simple control structure, and robustness against parameter variations are some of the features that lead to its popularity. However, original DTC suffers from major drawbacks namely high sampling requirements for digital implementation, high torque ripple [1], and low speed problem due to flux magnitude droops [2]. Since its first introduction in 1980's [3], two main groups of DTC variations have emerged to partially or fully solve these problems which can be classified as: 1) Non-Lookup table based DTC (NLT-DTC) and 2) Lookup table based DTC (LT-DTC).

For the NLT-DTC scheme, two approaches are employed mainly to reduce the torque ripple and switching frequency. The first one, which is one of the popular variations of DTC [4-6], is based on space vector modulation (SVM) denoted as DTC-SVM. As apposed to the LT-DTC whereby the voltage vectors are obtained from the look-up table, in NLT-DTC, the reference voltage vectors are generated from the control algorithm. The reference voltage vectors are then synthesized using a space vector modulator. One major drawback of this scheme is the increased complexity of its control structure and implementation. Fast processors are required to ensure small sampling period hence obtaining good control bandwidth. The second approach to the NLT-DTC is known as predictive torque control (PTC) which has gained considerable amount of attention recently [7-10]. Several implementations of PTC still exploit the hysteresis comparators of flux and torque as in the classical DTC, but the selection of voltage vectors is obtained through a predefined cost function rather than a lookup table. In general, PTC strategies suffer from total harmonic distortion and high computation burden [10]. For proper operation of NLT-DTC, appropriate control bandwidth must be ensured; this translates for the requirement of high performance processor. Furthermore, stable operation at very low speed and zero is not guaranteed in NLT-DTC, particularly under no loading conditions.

In the second group of DTC variations, which is the LT-DTC, a lookup table is used to select the switching states of inverter depending on flux and torque requirements. In principle, the schemes under this category operate based on the originally proposed DTC [3] , but with some modifications either in its control structure or in the look-up table. Various techniques with larger lookup tables have been reported in the literature [11-13] with good torque performance but resulting in higher complexity and therefore higher computational requirement. An alternative approach is the variation of hysteresis bands for the torque controller based on different speed profiles [14, 15]. Despite the simplicity of this method, which is focused mainly on achieving constant switching frequency, other major problems of DTC, such as high torque ripple and problems at low speed operations still exist. Other

This work was supported by the Basic Science Research Program through the National Research Foundation of Korea (NRF) funded by the Ministry of Science, ICT and Future Planning (2016R1A2B4010636).

I. M. Alsofyani and K. B. Lee are with the Department of Electrical and Computer Engineering, Ajou University, Suwon 16499, South Korea (e-mail: alsofyani@ajou.ac.kr; kyl@ajou.ac.kr).

N.R.N. Idris is with the Faculty of Electrical Engineering, Universiti Teknologi Malaysia, Johor Bahru 81310, Malaysia (e-mail: nikrumzi@ieee.org)

This article has been accepted for publication in a future issue of this journal, but has not been fully edited. Content may change prior to final publication. Citation information: DOI 10.1109/TPEL.2017.2773129, IEEE Transactions on Power Electronics

attempts [16, 17], have been carried out by injecting high-frequency triangular signals into the torque errors; this method is called the dithering technique. However, it generates an unpredictable switching frequency since the torque slopes that determine the frequency of the torque controller varies according to the operating conditions. Generally, the low speed performance offered by these solutions is not satisfactory as compared to the NLT-DTC category.

Recently, it is reported that the state estimation at low and zero speed of a DTC drive can be significantly improved by improving the flux regulation [18]. Based on the analysis performed in this work, it is shown that the stator flux regulation of LT-DTC drive at low and zero speed degraded due to the selection of the zero voltage vectors, which is used to reduce the torque. Since the flux cannot be properly regulated, stator current becomes distorted and the magnitude reduces such that the coupling between the stator and rotor circuits is lost. As a result of this, a fundamental model based state estimator, will perform unsatisfactorily at low and zero speed. It is shown that flux regulation can be significantly improved by selecting reverse voltage vectors instead of zero vectors whenever torque needs to be reduced. The selection of reverse voltage vectors at low speed in [18] is performed by using the constant switching frequency controller (CSFC). However, in order for the CSFC to function properly the PI controller (within the CSFC) has to be carefully designed. Furthermore, the frequency of the triangular wave sets a limit to the torque loop bandwidth, thus reducing the dynamic torque response when compared to the conventional DTC at regulated flux [19].

This work attempts to provide further analysis on flux droop in between flux sectors and flux degradation at low and zero speed. In addition, the idea of improving the state estimation by improving the flux regulation at low speed is extended to the classical DTC without replacing the hysteresis torque controller. The proposed method retains the conventional DTC algorithm, but with a minor modification to dynamically alter the amplitude of torque hysteresis band. In this way, the selection of reverse voltage vectors whenever torque needs to be reduced can be easily implemented by narrowing the hysteresis band based on a flux error range. Owing to the discrete sampling implementation, overshoot in the torque will touch the upper hysteresis band instead of the reference torque because of the narrow band. However, due to the selection of the reverse voltage vectors, torque ripple will be increased. Therefore, in order to avoid high torque ripple across the wide speed operation, the width of the hysteresis band will only be reduced whenever the flux regulation fails. In this paper, a dynamic hysteresis torque band (DHTB) is introduced to achieve a compromise solution between high torque ripple and effective flux regulation. The DHTB is used to select between two sets of torque hysteresis bands: the first set of hysteresis band width is based on 10-15% of rated torque [20, 21] in order to reduce current harmonics and torque ripple, whereas the second set is based on the torque hysteresis band width that will force the selection of reverse voltage vectors. The DTC drive will operate normally based on the first set of hysteresis band and will switch to the second set of hysteresis band once the flux regulation fails. By utilizing this technique, flux regulation problem at low speed is rectified without requiring any modification to the structure of DTC. Two types of DHTB are proposed to achieve a proper flux regulation at low speed using defined flux error with respect to the rated flux. This will allow further investigation of the switching frequency of reverse voltage vectors on the speed sensorless DTC drive. In comparison to the solution that is based on CSFC [18], the proposed method produces better torque dynamic since it uses hysteresis comparator, which is known to have fast response and large control bandwidth. The effectiveness of the DHTB methods in improving the flux regulation, hence the state estimation at low and zero speed, is demonstrated with the help of extended Kalman filter (EKF) observer, as presented in [18]. Simulations and experimental results are presented to show and compare the effectiveness of the proposed DHTB schemes in the performance of DTC of IM.

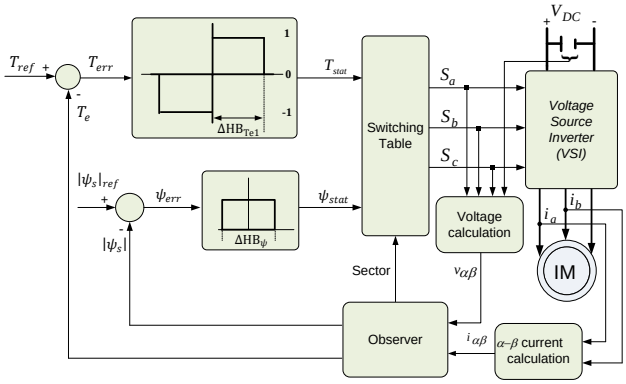

Fig.1. Initial structure of DTC of IM

II. Look-up Table Based DTC and State Estimation

A. Fundamentals of DTC of IM

The dynamic modeling of an induction machine can be described in terms of space vectors equations, which are expressed in the stator stationary reference frame as follows:

$$u_s = R_s i_s + \frac{d}{dt}\psi_s \tag{1}$$

$$0 = R_r i_r - j\omega_r \psi_r + \frac{d}{dt}\psi_r \tag{2}$$

$$\psi_s = l_s i_s + l_m i_r \tag{3}$$

$$\psi_r = l_r i_r + l_m i_r \tag{4}$$

$$T_e = \frac{3}{2} p \frac{l_m}{\sigma l_s l_r} |\psi_s||\psi_r| \sin\delta_{sr} \tag{5}$$

In these equations, i_s and i_r are the stator and rotor currents, ψ_s and ψ_r are the stator and rotor fluxes, ω_r is the rotor electric angular speed in rad/s, u_s is the stator voltage vector. R_s, R_r, l_s, l_r and l_m are the stator resistance, rotor resistance, stator self-inductance, rotor self-inductance, and mutual inductance, respectively. σ=1–$l_m^2 / l_s l_r$, p is the number of pole pairs, and δ_{sr} is the load angle between the stator and rotor fluxes.

This article has been accepted for publication in a future issue of this journal, but has not been fully edited. Content may change prior to final publication. Citation information: DOI 10.1109/TPEL.2017.2773129, IEEE Transactions on Power Electronics

Fig. 1 shows the original structure of Lookup-table-based DTC of induction machine, as proposed in [3]. The application of stator voltage vectors is based on the selection of the switching states (S_a, S_b, S_c) obtained from the lookup table, which are determined by the stator flux position (sector) and according to the demands of the torque and the stator flux to be increased (↑) or decreased (↓). The general rule of voltage selection based on the forward, zero, and reverse voltage vectors is depicted in Table I. The resultant states from the torque and flux hysteresis comparators are defined by T_{stat} (torque error status) and Ψ_{stat} (flux error status), respectively. The T_{stat} consists of three states: forward voltage vector (1), zero voltage vector (0), and reverse voltage vector (-1). Fig. 2 shows the two optimized voltage vectors for every sector, which are used to either increase or reduce the stator flux based on the flux and torque demands as given in Table I [3].

TABLE I
Selection of Voltage Vectors

Flux	Torque	Voltage vector selections	
↑	↓	Zero voltage vector	Reverse active voltage vector
	↑	Forward active voltage vector	
↓	↓	Zero voltage vector	Reverse active voltage vector
	↑	Forward active voltage vector	

B. State estimation of DTC variables

Although DTC itself is a speed-sensorless drive, most of the time, the rotor speed is still needed for speed control purposes. It is the objective of this paper to show the importance of the stator flux regulation in improving the performance of state estimators (rotor speed estimation, in particular). For this reason, an EKF-based observer that is used to estimate the rotor speed is implemented in this paper. The estimated speed is used as the feedback control signal for the closed-loop speed control scheme for the DTC drive. The observer also estimates rotor flux, which is then used to calculate the stator flux for the DTC algorithm. The structure of the EKF-based estimator implemented in this paper is similar to the structure of the previous work and is briefly explained in this section [18].

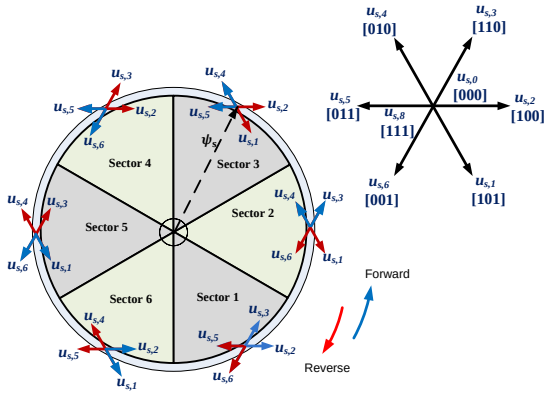

Fig. 2. The inverter outputs for each sector in forward and reverse operations

The mathematical model of the IM derived from (1) - (4) can be expressed in the (α,β) coordinate system. It is convenient to describe the induction machine model in state space matrix , which is given in the following general form [22].

$$\frac{d}{dt}x = f(x,u)+w \tag{6}$$

$$f(x,u) = Ax+Bu \tag{7}$$

$$z = Hx+v \tag{8}$$

where x is the state variables based on current model, u_s is the voltage vector, f is a differential function of x and u_s. A is the state process matrix, B is the input matrix, H is the observation matrix. z is the output vector. w and v are the system noise and measurement noise, respectively. Detailed description for the (6) to (8) are given as:

$$\underbrace{\frac{d}{dt}\begin{bmatrix} i_{s\alpha} \\ i_{s\alpha} \\ i_{s\beta} \\ \psi_{r\beta} \\ \omega_r \end{bmatrix}}_{x} = \underbrace{\begin{bmatrix} \frac{-\zeta}{\sigma l_s} & 0 & \frac{l_m}{\sigma l_r l_s \tau_r} & \frac{\omega_r l_m}{l_r l_s} & 0 \\ 0 & \frac{-\zeta}{\sigma l_s} & \frac{-\omega_r l_m}{l_r l_s} & \frac{l_m}{\sigma l_r l_s \tau_r} & 0 \\ \frac{l_m}{\tau_r} & 0 & \frac{-1}{\tau_r} & -\omega_r & 0 \\ 0 & \frac{l_m}{\tau_r} & \omega_r & \frac{-1}{\tau_r} & 0 \\ 0 & 0 & 0 & 0 & 0 \end{bmatrix}}_{A} \underbrace{\begin{bmatrix} i_{s\alpha} \\ i_{s\alpha} \\ i_{s\beta} \\ \psi_{r\beta} \\ \omega_r \end{bmatrix}}_{x} + \begin{bmatrix} \frac{1}{\sigma l_s} & 0 & 0 & 0 & 0 \\ 0 & \frac{1}{\sigma l_s} & 0 & 0 & 0 \end{bmatrix} \times \begin{bmatrix} u_{s\alpha} \\ u_{s\beta} \end{bmatrix} + w \tag{9}$$

$$\underbrace{\begin{bmatrix} i_{s\alpha} \\ i_{s\beta} \end{bmatrix}}_{z} = \underbrace{\begin{bmatrix} 1 & 0 & 0 & 0 & 0 \\ 0 & 1 & 0 & 0 & 0 \end{bmatrix}}_{H} \times \underbrace{\begin{bmatrix} i_{s\alpha} & i_{s\beta} & \psi_{s\alpha} & \psi_{s\beta} & \omega_r \end{bmatrix}^T}_{x} + v \tag{10}$$

where $\zeta = R_s + \frac{l_m^2}{l_r \tau_r}$

The procedure to obtain the estimated states using the EKF algorithm is described in the appendix. The stator flux in a stationary reference frame is calculated from the estimated rotor flux as follows:

$$\psi_{s\alpha} = \frac{l_m}{\tau_r}\psi_{r\alpha} + l_\sigma i_{s\alpha} \tag{11}$$

$$\psi_{s\beta} = \frac{l_m}{\tau_r}\psi_{r\beta} + l_\sigma i_{s\beta} \tag{12}$$

The electromagnetic torque is calculated in terms of stator flux and the measured stator current:

This article has been accepted for publication in a future issue of this journal, but has not been fully edited. Content may change prior to final publication. Citation information: DOI 10.1109/TPEL.2017.2773129, IEEE Transactions on Power Electronics

$$T_e = \frac{3}{2} p\left(\psi_{s\alpha} i_{s\beta} - \psi_{s\beta} i_{s\alpha}\right) \quad (13)$$

The voltage vectors, $u_{s\alpha}$ and $u_{s\beta}$ can be reconstructed from the switching states obtained from the lookup table, Sa, Sb, and Sc (which can be either 0 or 1) as given by:

$$u_{s\alpha} = \frac{1}{3} V_{DC}\left(2S_a - S_b - S_c\right) \quad (14)$$

$$u_{s\beta} = \frac{1}{\sqrt{3}} V_{DC}\left(S_b - S_c\right) \quad (15)$$

III. Effect of Hysteresis Torque Band on Flux Regulation

Owing to the discrete implementation of the DTC algorithm, the width of the hysteresis torque band (HTB) has to be appropriately selected and the sampling period should be as small as possible. The DTC is usually operated with nominal HTB (denoted as ΔHB_{Te1}) which is normally set between 10-15% of the rated torque [20] to ensure that the reverse voltage vectors (see Table I) as a result of overshoot (i.e. when the estimated toque exceeds the upper band) will not be selected during the torque reduction. This means that when torque needs to be reduced, zero voltage vectors are selected. This scenario can be shown in Fig. 3. The reverse voltage vectors are not selected to avoid high switching frequency of the voltage source inverter (VSI) as well as to ensure low torque ripple [20].

From (1), the rate of change in stator flux expressed in stationary reference frame is given as:

$$\frac{d}{dt}\psi_s = u_s - R_s i_s \quad (16)$$

If a small change in time Δt_s is considered, (16) can be written as

$$\Delta\psi_{s1} = \left(u_s - i_s R_s\right)\Delta t_s \quad (17)$$

Normally, in order to simplify the selection of voltage vectors, $i_s R_s$ is assumed to be small and hence neglected, thus (17) can be approximated as $\Delta\psi_{s1} \simeq u_s \Delta t_s$. If torque needs to be reduced, zero voltage vector is selected and according to this approximation, $\Delta\psi_{s1} = 0$ the stator flux halts. In practice, such assumption is acceptable if the speed is at medium and high-speed range; however, it is not valid at low speed when stator resistance drop is more pronounced.

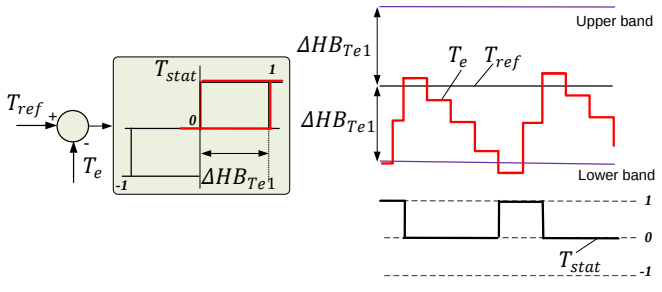

(a) (b)

Fig. 3. The normal behavior of discretized waveforms of torque in three-level hysteresis comparator with nominal torque hysteresis band

By considering the ohmic drop, the change in flux during the selection of zero voltage vectors becomes:

$$\Delta\psi_{s2} = \left(-i_s R_s\right)\Delta t_s \quad (18)$$

Fig.4 shows simulation results of a typical DTC drive system when speed steps to low frequency range (5 rad/s). The waveforms from top to bottom are the reference and estimated speeds (denoted as Ref. and Est., respectively), stator flux (ψ_s) electromagnetic torque (T_e), torque error (T_{err}), and output of hysteresis torque comparator (T_{stat}). The hysteresis torque band in this case is set to 1 Nm. As can be seen from the figure, during the zero-voltage vector selection (T_{stat} = 0), the flux magnitude reduces by $|\Delta\psi_{s2}|$. Since in this particular example $\Delta\psi_{s1} < \Delta\psi_{s2}$, the flux reduces rather than increases. This condition normally occurs at low speed under light load whereby the rate of change of increasing torque (S_t^+) is much higher than the rate of change of decreasing torque (S_t^-); this causes the duration of zero vector selection to be longer than the duration of the active voltage vectors.

Generally, S_t^+ and S_t^-, which are also defined as the positive and negative torque slopes, are expressed by [21]:

$$S_t^+ = -T_e\left(\frac{1}{\sigma\tau_s} + \frac{1}{\sigma\tau_r}\right) + \frac{3}{2}\frac{p}{2}\frac{l_m}{\sigma l_s l_r}\left(u_s - j\omega_r\psi_s\right) j\psi_r \quad (19)$$

$$S_t^- = -T_e\left(\frac{1}{\sigma\tau_s} + \frac{1}{\sigma\tau_r}\right) - \frac{3}{2}\frac{p}{2}\frac{l_m}{\sigma l_s l_r}\left(j\omega_r\psi_s\right) j\psi_r \quad (20)$$

From equations (19) and (20), there are three main variables, which can affect the torque slopes and contribute to the flux regulation: i) electrical torque (T_e), which depends on the step change of speed and machine loading, ii) motor rotor speed (ω_r), and iii) stator voltage vector (u_s). The two factors; i) and ii) can affect greatly the rate of change of decreasing torque (S_t^-) as shown in Fig. 4.

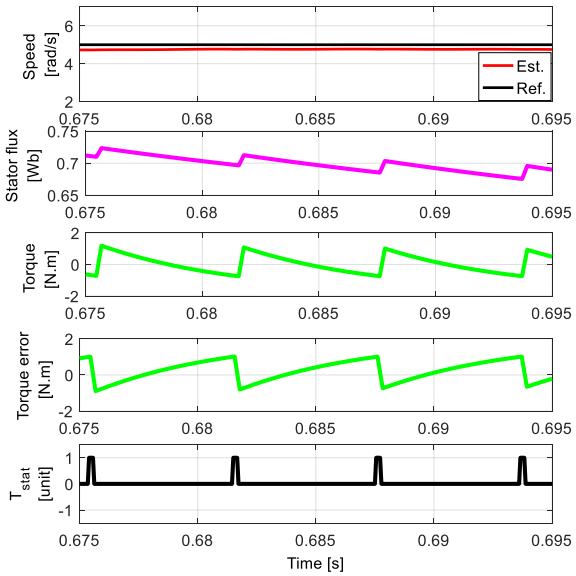

Fig. 4. Flux droop at low speed for DTC with nominal torque hysteresis band

This article has been accepted for publication in a future issue of this journal, but has not been fully edited. Content may change prior to final publication. Citation information: DOI 10.1109/TPEL.2017.2773129, IEEE Transactions on Power Electronics

The third factor; iii) on the other hand, contributes to the change rate of increasing torque (S_t^+). Note that tangential and radial components of the stator voltage vectors (u_s) are responsible for the behavior of the dynamics of torque and flux, respectively (the tangential and radial components of a voltage vector are defined as the components which are tangential and perpendicular to the circular locus of the stator flux, respectively). As the flux rotates, the magnitudes of tangential and radial components change with stator flux position. Fig. 5 shows the tangential and radial components variation for voltage vectors $u_{s,4}$ and $u_{s,5}$ at low speed and under light load as the flux enters, reaches halfway, and leaves sector 3. When the flux in sector 3, voltage vectors $u_{s,4}$ and $u_{s,5}$ are used to increase and reduce the flux respectively. Both $u_{s,4}$ and $u_{s,5}$ will, at the same time, increase the torque. Upon entering sector 3, the radial component of $u_{s,4}$ (designated as $u_{s,4\beta}$) is very weak.

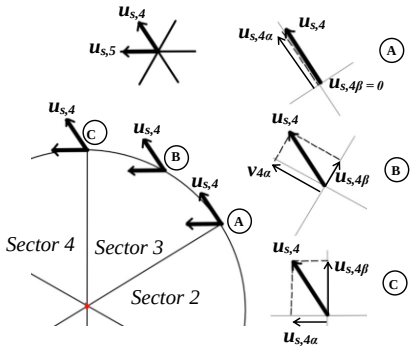

Fig. 5. Variations of the radial and tangential components of voltage vector ($u_{s,4}$) through sector 3

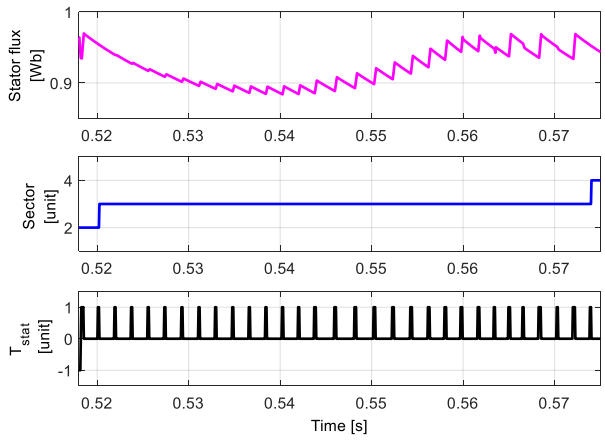

Fig. 6. Simulation results for the effects of radial and tangential components of voltage vector on flux regulation through sector 3

On the other hand, $u_{s,4}$ has a strong torque component (designated as $u_{s,4\alpha}$). Under this condition the flux fails to increase since the duration of active voltage vector is too short and furthermore, the increment in flux when $u_{s,4}$ is selected is very small; as a result, $\Delta\psi_{s1} < \Delta\psi_{s2}$. When the flux moves half-way of sector 3, the radial component of the voltage vector $u_{s,4}$ becomes stronger and its tangential component becomes weaker, hence the flux increases. However, if the speed is too low, the flux cannot be increased, and the flux controller completely fails. The weakening followed by strengthening of radial component across a sector subsequently causes the stator flux droop at the middle of a sector and this is undesirable since it leads to deterioration in the stator currents and causes additional current harmonics [23].

To illustrate this, simulation results of a typical DTC when the motor speed runs at 10 rad/s is shown in Fig. 6. The top trace shows stator flux magnitude, followed by the sector number and the torque hysteresis comparator output, T_{stat}. The results clearly indicate the droop in the stator flux which begins at the start of the sector due to i) weak radial component of the voltage vector, ii) shorter duration of active voltage vector due to the strong tangential component of voltage vector, and iii) longer duration of zero voltage vector due to the low rate of change of decreasing torque. The flux drooping results in a non-circular flux locus hence reflected in the non-sinusoidal stator current, which also contains additional current harmonics.

With nominal band, ΔHB_{Te1}, stator flux regulation failure is likely to happen, and this will affect the performance of any drive system, which uses observer for state estimation. To substantiate this, in this paper, EKF, as presented in [17], is used to estimate the rotor speed. The reduction of stator flux below its rated value due to the failure in its regulation imposed significant effect to the estimated speed especially when the covariance filters of the EKF is tuned at the rated stator flux. Since the flux falls below its rated value, the state estimation will be degraded.

The problem of flux regulation can be removed if the magnitude of the flux is controlled by selecting suitable voltage vectors whenever the torque needs to be reduced. An effective way of achieving this is by reducing the width of the torque hysteresis band so that, owing to the overshoot in the torque due to the digital implementation, reverse voltage vectors are selected when the torque needs to be reduced. Fig. 7 shows the reduction in the hysteresis band (ΔHB_{Te2}) such that the overshoot in T_e (or undershoot in T_{err}) causes the selection of reverse voltage vector. By doing so, (18) now becomes

$$\Delta\psi_{s2} = \left(u_{s,r} - i_s R_s\right)\Delta t_s \tag{21}$$

and (20) is expressed as

$$S_t^- = -T_e\left(\frac{1}{\sigma\tau_s} + \frac{1}{\sigma\tau_r}\right) + \frac{3}{2}\frac{p}{2}\frac{l_m}{\sigma l_s l_r}\left(u_{s,r} - j\omega_r\psi_s\right)j\psi_r \tag{22}$$

where, $u_{s,r}$ is the reverse voltage vector. By selecting suitable reverse voltage vectors, $\Delta\psi_{s2}$ can be made to increase or decrease and, at the same time, since δ_{sr} in (5) reduces, torque will decrease. Fig. 8 shows the vector diagram of stator flux (at sector 3) and rotor flux rotating in counterclockwise direction. Two cases are considered, whereby (1) reverse voltage vector us,1 is selected to reduce the torque as well as to reduce the flux, and (2) reverse voltage vector us,2 is selected to reduce the torque and increase the flux. In each case, the torque angle δ_{sr} decreases ($\delta_{sr2} < \delta_{sr1}$) thus

This article has been accepted for publication in a future issue of this journal, but has not been fully edited. Content may change prior to final publication. Citation information: DOI 10.1109/TPEL.2017.2773129, IEEE Transactions on Power Electronics

according to (5), causes a torque reduction.

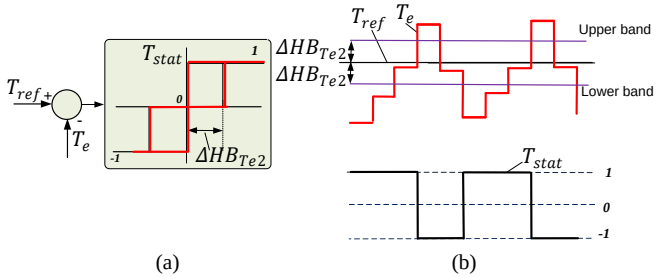

Fig. 7. Behavior of discretized waveform of torque in three-level hysteresis comparator with small torque hysteresis band.

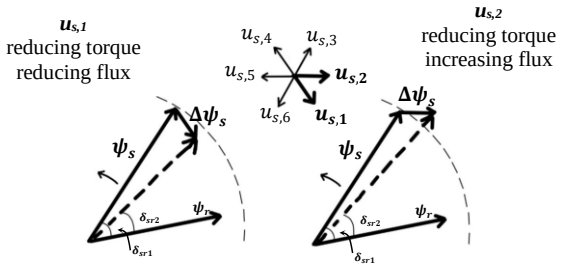

Fig. 8. Effects of selecting reverse voltage vectors to reduce or increase stator flux linkage at sector 3.

IV. Proposed Dynamic Hysteresis Torque Band

In order to accomplish a proper flux regulation at low motor speed operation and under light or zero load based on the discussion in Section III, the width of the HTB has to be reduced. To accomplish this, the band is reduced to 0.5 % of the rated torque, which roughly equals to 0.045 N.m based on the rating of the machine used in this paper; the reduced hysteresis band is referred as ΔHB_{Te2}. The application of ΔHB_{Te2}, however, is not desirable in the middle and high-speed range whereby flux can be regulated using ΔHB_{Te1}. Therefore, a compromise solution is proposed using a dynamic hysteresis torque band (DHTB) technique.

The DHTB is proposed to avoid the undesirable effects of reverse voltage vectors in the medium and high-speed regions and to solve the flux regulation problem at low and zero speed. In general, DHTB strategy switches hysteresis torque band from ΔHB_{Te1} to ΔHB_{Te2} whenever the stator flux regulation fails. In this paper, two DHTB schemes are proposed with the purpose of (i) improving flux regulation at low and zero speed thus enhancing the performance of the state estimator (EKF) and (ii) removing the flux drooping within a sector thus reducing current distortion. Two methods of DHTB are presented and compared, named as DHTB-I and DHTB-II.

A. DHTB-I

The first DHTB scheme utilizes the speed information directly either from encoder or observer as shown in Fig. 9. This method was previously proposed in our simulation work [24] and the activation of the ΔHB_{Te2} is based on certain range of low speed. The threshold speed that will activate ΔHB_{Te2} is determined offline by observing the critical point in which the flux regulation starts to degrade based on simulations or from experiments.

It is necessary to limit the critical flux error in order to simplify the selection between HTBs. Therefore, the condition of critical flux point for the selection between HTBs can be expressed using reference (rated) flux as:

$$\psi_c = k\left(\left|\psi_s\right|_{ref}\right) \tag{23}$$

where $\left|\psi_s\right|_{ref}$ is the magnitude of the reference flux, ψ_c is the critical flux point and k is the weighting factor in the range ($0 < k < 1$). In other words, the flux error (ψ_{err}) should not exceed the critical flux error (E_c) defined in (24).

$$E_c = \left|\psi_s\right|_{ref} - \psi_c \tag{24}$$

The value of k should be selected properly to avoid the activation of ΔHB_{Te2} in medium and high-speed range, which is undesirable. Increasing k results in the increase of flux critical point and avoidance of large degradation of flux. In contrast, with decreasing k, the flux error point will be smaller and hence large flux droop will occur before the activation of ΔHB_{Te2}. It is very difficult to find the weighting factor mathematically. Thus, a trial-and-error technique is used to obtain the proper gain of k value to ensure the selection of ΔHB_{Te2} at low speed region. In this paper, the flux regulation is considered to degrade when the weighting factor, k is set to 0.95; thus, $\psi_c = 0.9063\ Wb$ and $E_c = 0.0477\ Wb$.

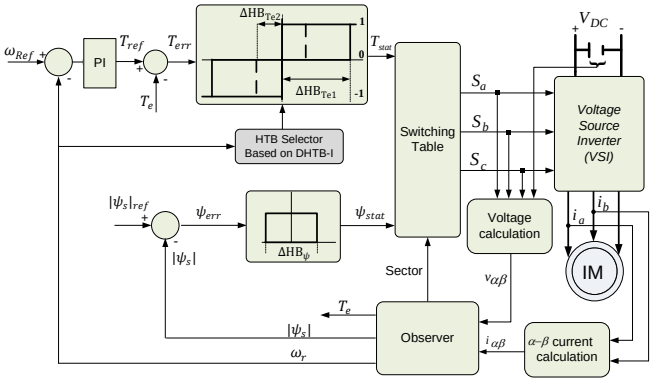

Fig.9. Structure of DTC-hysteresis-based induction machine with the proposed DHTB-I

The critical speed depends on the parameters of the motor and the mechanical load of the drive system. The worst-case condition is when the machine is unloaded because under this condition, the (negative) slope of the torque is extremely low, as previously described in section III. This in turn increases the duration of zero voltage vector application thus increases the possibility of $\Delta\psi_{s1} < \Delta\psi_{s2}$ (see Fig. 4). Therefore, the DHTB-I will operate based on the following condition:

$$HTB = \begin{cases} \Delta HB_{Te1}, & for\ \left|\omega_r\right| > \left|\omega_r^{\psi c}\right| \\ \Delta HB_{Te2}, & for\ \left|\omega_r\right| \le \left|\omega_r^{\psi c}\right| \end{cases} \tag{25}$$

Where $\omega_r^{\psi c}$ is the critical (threshold) speed with respect to critical flux point. Based on the simulation and experiment for

This article has been accepted for publication in a future issue of this journal, but has not been fully edited. Content may change prior to final publication. Citation information: DOI 10.1109/TPEL.2017.2773129, IEEE Transactions on Power Electronics

the machine used in this paper, $\omega_r^{\psi c} \approx 12\ rad/s$.

B. DHTB-II

In the second method, the activation of ΔHB_{Te2} is determined directly from the magnitude of stator flux error. Unlike the previous method, the speed information is not needed, as shown in Fig. 10. Thus, the condition used to determine DHTB-II operation is given in the following equation:

$$HTB = \begin{cases} \Delta HB_{Te1}, & for\ \psi_{err} < E_c \\ \Delta HB_{Te2}, & for\ \psi_{err} \geq E_c \end{cases} \quad (26)$$

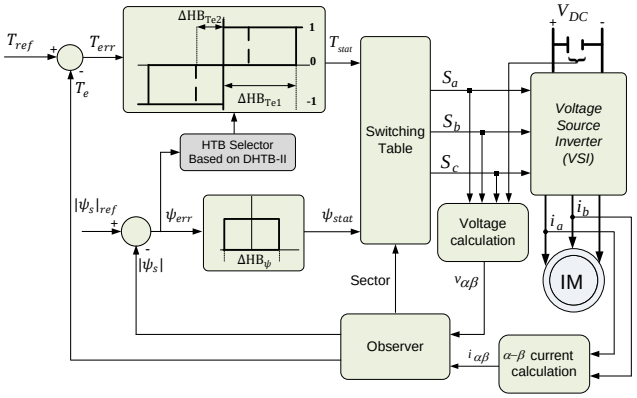

Fig.10. Structure of DTC-hysteresis-based induction machine with the proposed DHTB-II.

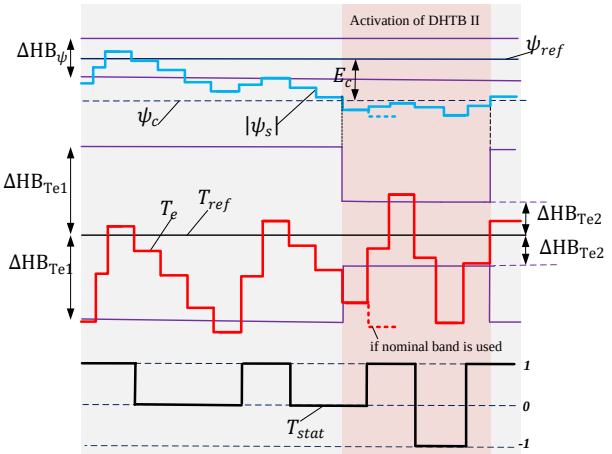

Fig.11. An example of discretized waveforms of flux, torque, and torque status during the dynamic of the hysteresis torque band with DHTB-II method

There is a possibility that there will be a high frequency alternate switching between ΔHB_{Te1} and ΔHB_{Te2}, which is limited by the sampling frequency of the control system. Note that the selection of ΔHB_{Te2} will either reduce the time duration of the applied zero voltage vector, or introduce a torque overshoot to select reverse voltage vector for rapid torque reduction as illustrated in Fig. 11, which is used as an example. For this reason, the selected voltage vectors will contain a mixture of forward active, zero, and reverse active voltage vectors whenever the flux is regulated at this threshold value.

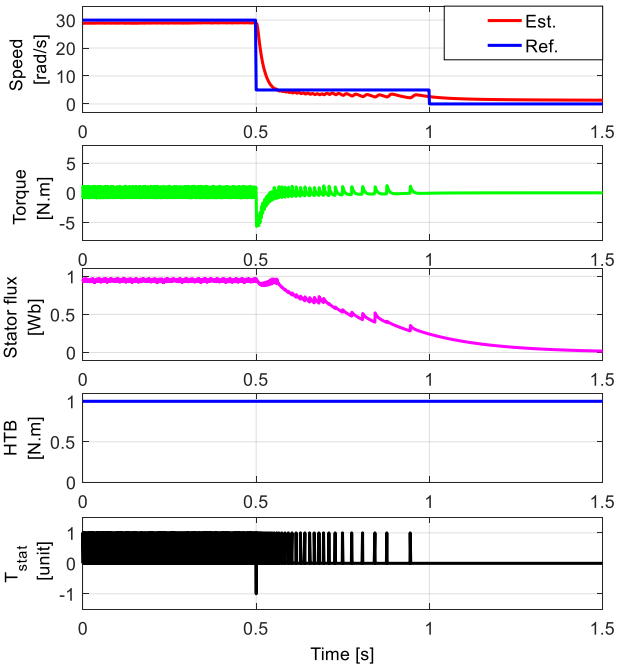

Fig.12. Simulation results of IM for DTC with nominal HTB

V. Simulation Results

To validate the effectiveness of the proposed dynamic hysteresis torque band, some simulations are carried out in the DTC-hysteresis-based induction motor using a MATLAB/SIMULINK software package. The system parameters and DTC values are as shown in Table II. It should be noted that the simulation does not include the inverter nonlinearities due to dead-time effect and whole motor model dynamics. For clarity, reference speed, estimated speed, and torque hysteresis band are abbreviated with Ref., Est., and HTB, respectively.

TABLE II
Induction Machine Parameters and DTC Values

Induction Machine	
Rated power	1.5 kW
Rated voltage	400 V
Rated current	3.7 A
Rated speed	1430 rpm
Efficiency	82.8 %
Power factor	0.72
Stator resistance	3 Ohm
Rotor resistance	4.1 Ohm
Stator self-inductance	0.3419 H
Rotor self-inductance	0.3513 H
Mutual inductance	0.324 H
Number of pole pair	2
DTC Values	
Torque hysteresis band (nominal), ΔHB_{Te1}	1 Nm
Torque hysteresis band (reduced), ΔHB_{Te2}	0.045 Nm
Flux hysteresis band, ΔHB_ψ	0.025 Wb
Rated torque	9 N.m
Rated stator flux	0.954Wb

Figs. 12, 13, and 14 show the waveforms of speed, torque, stator flux, torque hysteresis band, and torque status error during the medium, low, and zero-speed regions for sensorless

This article has been accepted for publication in a future issue of this journal, but has not been fully edited. Content may change prior to final publication. Citation information: DOI 10.1109/TPEL.2017.2773129, IEEE Transactions on Power Electronics

DTC system with the nominal HTB and the two proposed DHTB schemes. In these figures, HTB =1N.m indicates that ΔHB_{Te1} is used whereas HTB = 0.045 N.m indicates that ΔHB_{Te2} is selected. In all cases, the speed feedback is obtained from the estimated speed based on EKF.

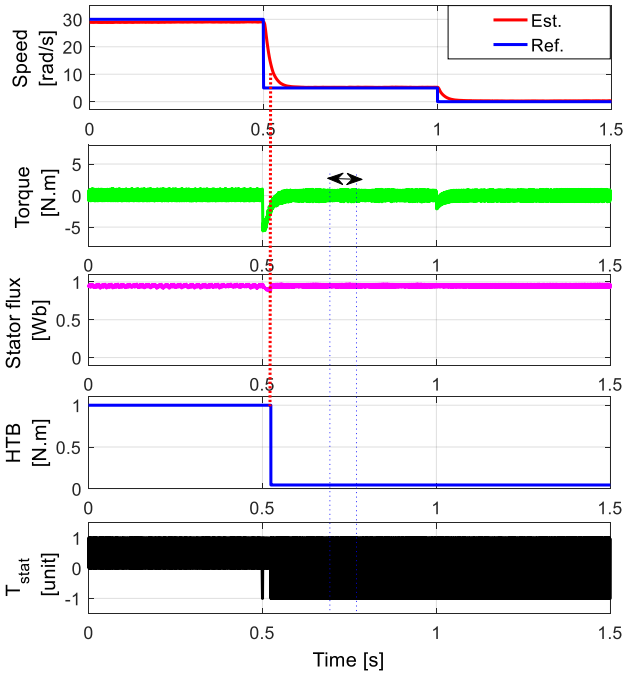

Fig.13. Simulation results of IM for DTC with DHTB-I

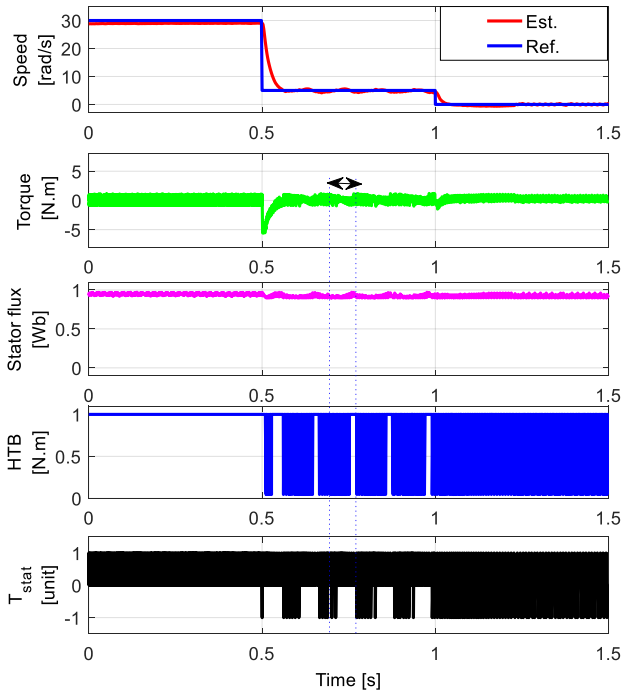

Fig.14. Simulation results of IM for DTC with DHTB-II

It is seen from Fig. 12 that the DTC with ΔHB_{Te1} (1 N.m) shows very poor performance due to the deterioration of flux regulation, especially when the motor speed steps to zero rad/s. On the other hand, when DHTB schemes are applied as shown in Figs. 13 and 14, the state estimation of speed and torque is improved owing to the proper flux regulation.

It can be observed from the DTC with DHTB-I in Fig. 13 that once the motor speed reaches 12 rad/s, the ΔHB_{Te2} (0.045 N.m) is selected resulting in forward and reverse vector selections as indicted by the torque error status. However, Fig. 14 shows that DTC with DHTB-II does not operate with fixed HTB.

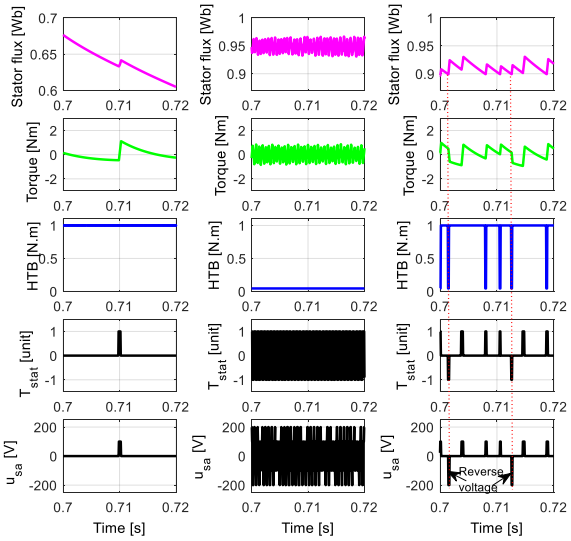

Fig.15. Zoomed images for the low speed operation of IM for (a) DTC with nominal HTB, (b) DTC with DHTB-I, and (c) DTC with DHTB-II

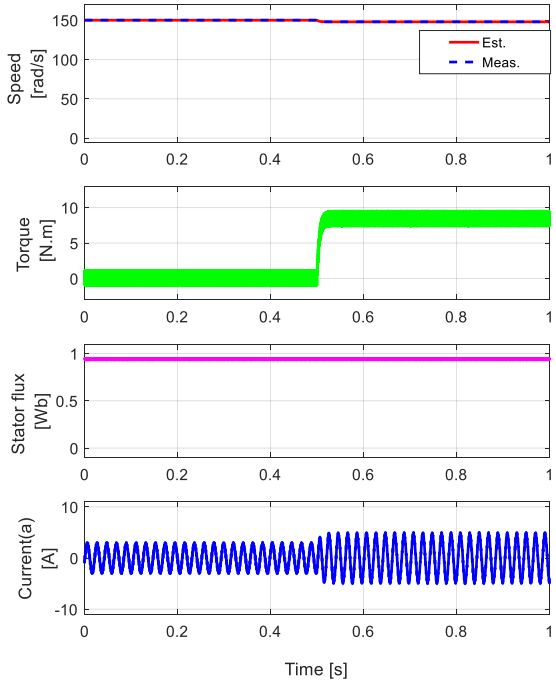

Fig.16. Simulation results of IM for DTC with nominal HTB at rated speed under rated load torque disturbance

For clearer picture, part of the data in the region between the double arrow "↔" for Figs. 12, 13, and 14 with the corresponding stator voltage (u_{sa}) are zoomed in Fig. 15. Although the DHTB-I can offer superior performance of regulating flux to its rated or reference value as shown in Fig.

This article has been accepted for publication in a future issue of this journal, but has not been fully edited. Content may change prior to final publication. Citation information: DOI 10.1109/TPEL.2017.2773129, IEEE Transactions on Power Electronics

15b, this scheme produces very high switching of voltage due to non-selection of zero vectors and hence results in poor efficiency. As can be seen from Fig. 15c, the selection between ΔHB_{Te1} and ΔHB_{Te2} keeps alternating whenever the flux error ψ_{err} goes below and above the critical flux error E_c of 0.0477 Wb, as discussed previously. This is the reason why the selection of zero vectors can be seen whenever the flux is regulated above the critical value. Though, DHTB-II cannot reach the rated flux at very low speed, it can offer less switching frequency of voltage, and hence improved efficiency.

The response to external load disturbance is illustrated in Figs. 16 for the classical DTC. At t = 0.5s, the load is suddenly changed from 0 (no-load) to 9 Nm (full-load) at 150 rad/s. The speed-senesorless DTC drive shows good rejection to the load disturbance. It is also observed that the flux is well-regulated under light and rated load. It is worth noting that since the stator flux is stable at the rated speed, the DTC will operate at the nominal hysteresis torque band ΔHB_{Te1} and therefore, both DHTB methods will be deactivated at this speed region.

VI. Implementation and Experimental Results

To verify the proposed system, a laboratory-scale DTC of IM drive as shown in Fig. 17 is constructed. The experimental set-up consists of a two-level inverter and a 1.5-kW squirrel-cage induction motor coupled to a hysteresis brake to provide a mechanical load, which is controlled using a proportional amplifier. The control system and EKF observer are implemented using the dSPACE 1104 controller board and Xilinx field-programmable gate array (FPGA) (Basys2 board

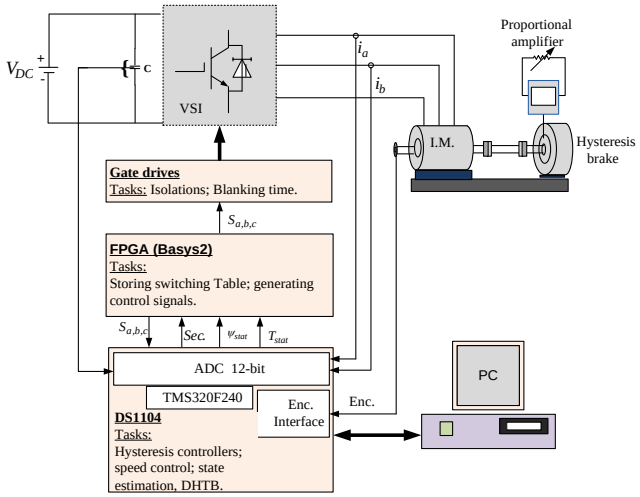

Fig.17. Functional block diagram of the experiment set-up

from digilent). The main tasks of the FPGA are to store the switching table of DTC and to generate and feed the three control signals to the two-level inverter. The sampling period of the DTC with EKF observer, containing the proposed dynamic hysteresis torque band, is 55 µs. An incremental encoder with 1024 PPR is used to measure the rotor speed for comparison purposes, which is sampled for every 10 ms. The speed feedback for the closed-loop speed control is obtained from the EKF estimator. For safety reason, the DC link voltage is limited to 300 V, which means that the base speed is reduced to 76 rad/s. Estimated speed, measured speed, stator flux, and torque, and other corresponding control signals are observed and recorded using the ControlDesk software that comes with dSPACE 1104. The threshold speed $\omega_r^{\psi c}$ which corresponds to the critical flux point ψ_c is experimentally found to be approximately at 12 rad/s.

At first, the effect of load torque on flux regulation is investigated on DTC with the nominal hysteresis torque band, ΔHB_{Te1} at low speed. Fig. 18 shows the behavior of estimated speed, measured speed, torque, stator flux, and torque hysteresis band for the conventional DTC, when the motor speed steps down from 15 rad/s to 5 rad/s. From Fig. 18, it is clearly seen that flux regulation suddenly deteriorated once the speed drops to low speed (5 rad/s). The reason is that the negative torque slope reduces causing long duration of zero voltage vectors as shown in the zoomed segment (4.0s to 4.01s) due to the low magnitude of speed and light load. According to equation (20) and our analysis in Section III, the negative torque slope can be increased by applying load torque disturbance on the motor, which can result in shortening zero voltage vectors. Therefore, after applying a load toque (2 N.m.) at t = 6.3s, the negative torque slopes increase (see the zoomed segment from 10.0s to 10.1s) resulting in shorter zero voltage vectors, and hence higher torque switching. It is worth noting that both zoomed segments before and after the load disturbance have the same time duration. Consequently, the stator flux starts rectifying slowly towards the rated (reference) flux and hence improving the flux regulation.

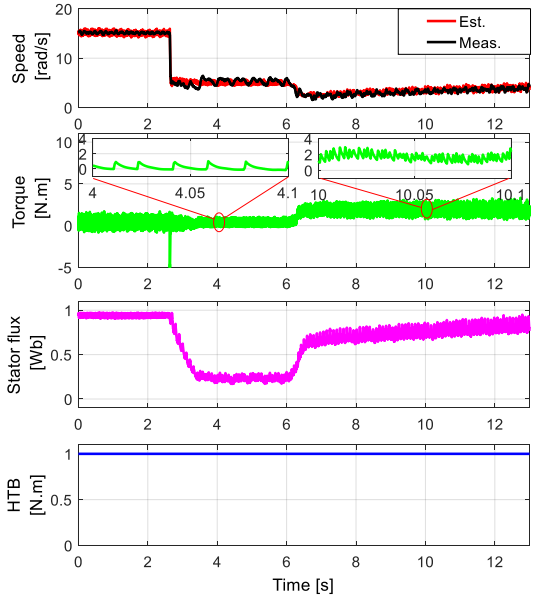

Fig.18. Experimental results for low speed operation with step change load torque for conventional DTC

Next, the behavior of the estimated speed, measured speed, torque dynamic, and measured currents (phase “a” and “b”) in the conventional DTC and the proposed DTC schemes are investigated by applying a step change of speed reference from zero rad/s to the base speed (76 rad/s) at 0.5 s as shown in Figs. 19 ,20, and 21, respectively. It can be seen in Fig. 19, for the conventional DTC, during zero speed operation, the

This article has been accepted for publication in a future issue of this journal, but has not been fully edited. Content may change prior to final publication. Citation information: DOI 10.1109/TPEL.2017.2773129, IEEE Transactions on Power Electronics

flux regulation completely fails. When a step speed reference is introduced, the flux starts to build-up and since the flux does not reach its rated value yet, the speed is inaccurately estimated. This faulty speed information causes an incorrect torque reference to be produced by the speed controller and subsequently, high surge in the starting current close to 9 A is observed. For both the proposed dynamic hysteresis torque bands shown in Figs. 20 and 21, the flux is established even before a step speed reference is introduced; hence the state variables of speed and torque are properly estimated, and the starting current becomes less than 5 A.

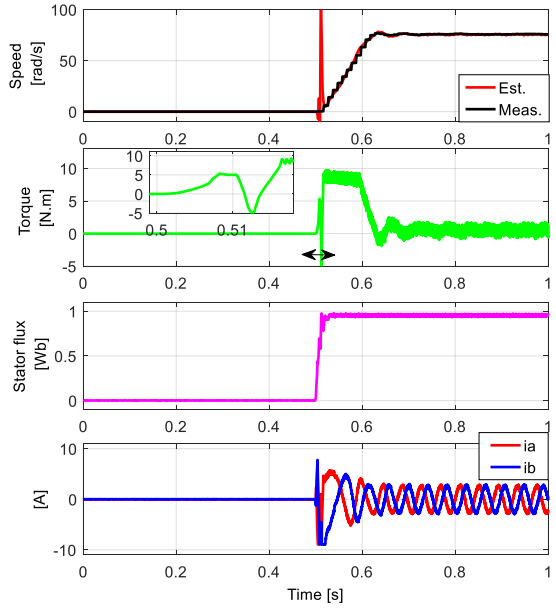

Fig.19. Experimental results for the starting response of IM from zero to base speed for conventional DTC

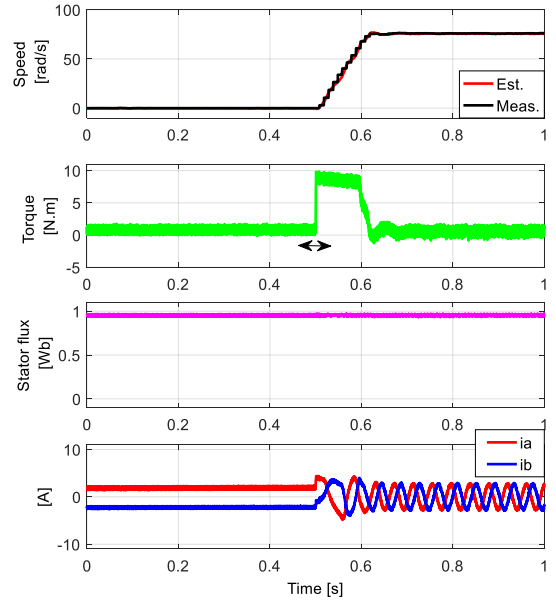

Fig.20. Experimental results for the starting response of IM from zero to base speed for DTC with DHTB-I

For the purpose of better comparison between DHTB-I and DHTB-II, the data taken for the torque (i.e., marked with "↔" in Figs. 20 and 21) are plotted with the corresponding torque error status, T_{stat}, and HTB shown in Fig. 22. It can be observed that both control algorithms show fast instantaneous torque dynamics from zero speed command. From the torque error status in Fig. 22a, it is seen there is very high switching of forward and reverse voltage vectors with no zero-voltage vector selection before and after the step change of torque. As discussed earlier, due to the selection of ΔHB_{Te2} that is based on speed, DHTB-I will continuously use ΔHB_{Te2} as long as the speed is less than the threshold speed of 12 rad/s.

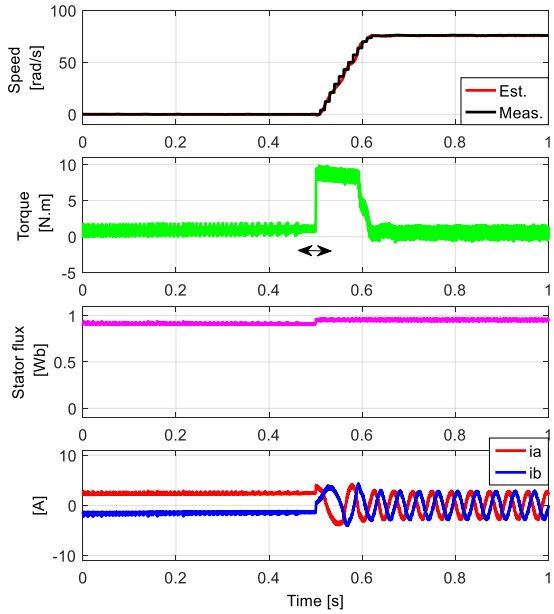

Fig.21. Experimental results for the starting response of IM from zero to base speed for DTC with DHTB-II

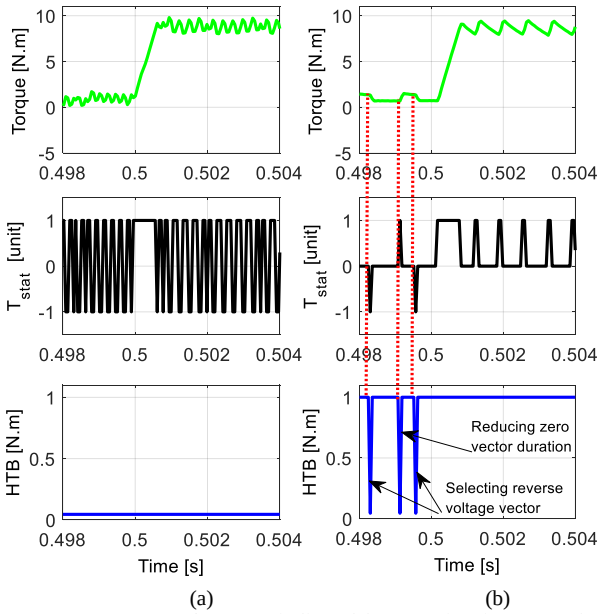

Fig.22. Zoomed area of Torque indicated by "↔" in Figs. 20 and 21 for starting operation and the corresponding torque error status and hysteresis torque bands for (a) DTC with DHTB-I and (b) DTC with DHTB-II.

The DHTB-II will either reduce the zero-vector duration or introduce a reverse voltage vector due to the switching between ΔHB_{Te1} and ΔHB_{Te2} as clearly seen in Fig. 22b. It is also shown that negative torque slope becomes much

This article has been accepted for publication in a future issue of this journal, but has not been fully edited. Content may change prior to final publication. Citation information: DOI 10.1109/TPEL.2017.2773129, IEEE Transactions on Power Electronics

steeper after the step change of torque without selecting ΔHB_{Te2} (0.045 N.m), although the estimated speed has not exceeded 1 rad/s yet. This is in agreement with our discussion in Section III that the increase in T_e causes a proportional increase in the torque slope.

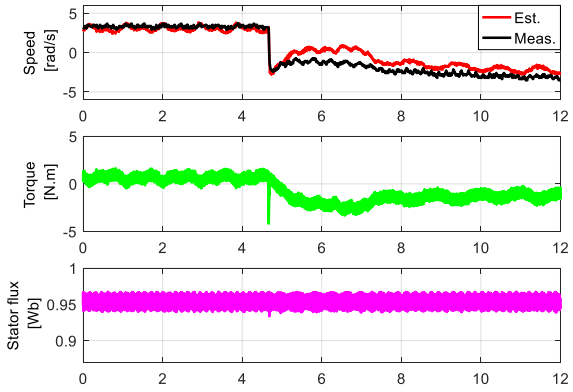

Fig.23. Experimental results for the low speed of IM in forward and reverse motoring for DTC with DHTB-I

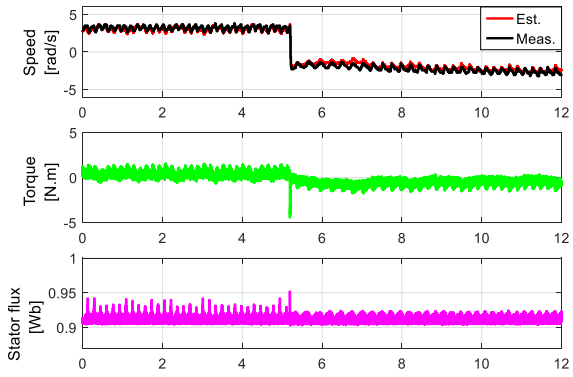

Fig.24. Experimental results for the low speed of IM in forward and reverse motoring for DTC with DHTB-II

Finally, Figs. 23 and 24 illustrate the performance for both DHTB schemes at low speed in forward and reverse motor directions. In both methods, the speed reference is reversed from 3 to −3 rad/s at no load. It is obvious in Fig.23 that the stator flux is regulated to its rated value based on the DTC with DHTB-I. However, it is observed that the torque and speed based on this scheme have large fluctuations and the estimated speed has poor tracking capability with higher speed errors; particularly when the speed is reversed. This is because the dead-time effect becomes more significant as a result of non-zero vector selection resulting in rapid change of torque [25] and higher switching frequency as shown in Fig. 22a. This behavior doesn't exist in the simulation results since the dead-time effect was not considered. On the other hand, in Fig. 24 it is seen that the torque waveform in DTC with DHTB-II is more stable with reduced oscillations, even though, the stator flux is not regulated to rated value. Consequently, there is a relative improvement in the estimated speed, which has also better tracking capability to the speed command.

VII. Conclusion

In this paper, two schemes of a simple dynamic hysteresis torque band namely; DHTB-I and DHTB-II are proposed to improve the flux regulation in DTC-hysteresis-based induction machine at low speed range. The working principle of both DHTB schemes depends on the selection of the hysteresis torque band based on a defined flux error to solve the low speed problem of DTC. Both DHTB schemes offer excellent speed startup and torque dynamic from zero speed, as well as solving the large starting current. However, compared to DTC with DHTB-I, DTC with DHTB-II shows better estimated torque and speed performances at low speed due to the reduction of switching frequency of inverter. The main advantage of the proposed method is its simplicity since it doesn't require any modification to the conventional DTC structure. Simulation and experimental results were presented to compare and verify the effectiveness of the proposed DHTB schemes.

VIII. Appendix

The stochastic continuous time system must be expressed in the discrete form in order to fit with the structure of extended KF (EKF). Assuming the system noise and the measurement noise as zero-mean white noises, the recursive EKF equations are performed in two stages, prediction ((27) - (30)) and update ((31) - (32)).

$$x_{k+1} = f(x_k, u) + w_k \tag{27}$$

$$f(x_k, u_k) = Ax_k + Bu_k \tag{28}$$

The linearization of (24) is performed around the current estimated state vector x_k as given in (25).

$$F_k = \frac{\partial}{\partial x_k} f(x_k, u_k)\Big|_{x_k} \tag{29}$$

This allows for obtaining the remaining of EKF algorithm as below:

$$P_{k+1/k} = F_k P_{k/k} F_k + Q \tag{30}$$

$$K_{k+1/k} = HP_{k+1/k} / \left(H P_{k+1/k} H^T + R\right) \tag{31}$$

$$x_{k+1/k+1} = x_{k+1/k} + K_{k+1}\left(z_k - H x_{k+1/k}\right) \tag{32}$$

$$P_{k+1/k+1} = \left(I - K_{k+1}H\right) P_{k+1/k} \tag{33}$$

where P is the covariance matrix of state estimation error, Q is the process covariance, and R is the measurement covariance. K is the correction term that is used to update the output received form prediction stage, and I denotes the diagonal unity matrix.

IX. References

[1] A. B. Jidin, N. R. B. N. Idris, A. B. M. Yatim, M. E. Elbuluk, and T. Sutikno, "A Wide-Speed High Torque Capability Utilizing Overmodulation Strategy in DTC of Induction Machines With Constant Switching Frequency Controller," *IEEE Trans. Power Electronics*, vol. 27, no. 5, pp. 2566-2575, 2012.

[2] G. S. Buja and M. P. Kazmierkowski, "Direct torque control of PWM inverter-fed AC motors - a survey," *IEEE Trans. Ind. Electronics*, vol. 51, no. 4, pp. 744-757, 2004.
[3] I. Takahashi and T. Noguchi, "A New Quick-Response and High-Efficiency Control Strategy of an Induction Motor," *IEEE Trans. Ind. App.*, vol. IA-22, no. 5, pp. 820-827, 1986.
[4] K. B. Lee and F. Blaabjerg, "Sensorless DTC-SVM for Induction Motor Driven by a Matrix Converter Using a Parameter Estimation Strategy," in IEEE Transactions on Industrial Electronics, vol. 55, no. 2, pp. 512-521, Feb. 2008.
[5] D. Casadei, G. Serra, and A. Tani, "Implementation of a direct control algorithm for induction motors based on discrete space vector modulation," *IEEE Trans. Power Electronics*, vol. 15, no. 4, pp. 769-777, 2000.
[6] A. H. Abosh, Z. Q. Zhu and Y. Ren, "Reduction of Torque and Flux Ripples in Space Vector Modulation-Based Direct Torque Control of Asymmetric Permanent Magnet Synchronous Machine," in IEEE Transactions on Power Electronics, vol. 32, no. 4, pp. 2976-2986, April 2017.
[7] J. Rodriguez *et al.*, "State of the Art of Finite Control Set Model Predictive Control in Power Electronics," *IEEE Trans. Ind. Informat.*, vol. 9, no. 2, pp. 1003-1016, 2013.
[8] Y. Cho, Y. Bak and K. B. Lee, "Torque-Ripple Reduction and Fast Torque Response Strategy for Predictive Torque Control of Induction Motors," in *IEEE Transactions on Power Electronics*, vol. PP, no. 99, pp. 1-1..
[9] W. Fengxiang *et al.*, "An Encoderless Predictive Torque Control for an Induction Machine With a Revised Prediction Model and EFOSMO," *IEEE Trans. Ind. Electron.*, vol. 61, no. 12, pp. 6635-6644, 2014.
[10] M. Habibullah, D. D. C. Lu, D. Xiao and M. F. Rahman, "Finite-State Predictive Torque Control of Induction Motor Supplied From a Three-Level NPC Voltage Source Inverter," in *IEEE Transactions on Power Electronics*, vol. 32, no. 1, pp. 479-489, Jan. 2017.
[11] C. Patel, R. P. P. A. Day, A. Dey, R. Ramchand, K. Gopakumar, and M. P. Kazmierkowski, "Fast Direct Torque Control of an Open-End Induction Motor Drive Using 12-Sided Polygonal Voltage Space Vectors," *IEEE Trans. Power Electronics*, vol. 27, no. 1, pp. 400-410, 2012.
[12] S. S. Sebtahmadi, H. Pirasteh, S. H. A. Kaboli, A. Radan, and S. Mekhilef, "A 12-Sector Space Vector Switching Scheme for Performance Improvement of Matrix-Converter-Based DTC of IM Drive," *IEEE Trans. Power Electronics*, vol. 30, no. 7, pp. 3804-3817, 2015.
[13] K. B. Lee, J. H. Song, I. Choy and J. Y. Yoo, "Improvement of low-speed operation performance of DTC for three-level inverter-fed induction motors," *IEEE Transactions on Industrial Electronics*, vol. 48, no. 5, pp. 1006-1014, 2001.
[14] H. I. Okumus and M. Aktas, "Direct Torque Control of Induction Machine Drives Using Adaptive Hysteresis Band for Constant Switching Frequency," in *Electric Machines & Drives Conference, 2007. IEMDC '07. IEEE International*, 2007, vol. 2, pp. 1762-1767.
[15] J. K. Kang, D. W. Chung, S. K. Sul, "Direct torque control of induction machine with variable amplitude control of flux and torque hysteresis bands," in *Electric Machines and Drives, 1999. International Conference IEMD '99*, 1999, pp. 640-642.
[16] M. P. Kazmierkowski and A. Kasprowicz, "Improved direct torque and flux vector control of PWM inverter-fed induction motor drives," *Trans. Ind. Electron*, vol. 42, pp. 344–350, Aug. 1995.
[17] T. Noguchi, M. Yamamoto, S. Kondo, and I. Takahashi, "High frequency switching operation of PWM inverter for direct torque control of induction motor," in *Industry Applications Conference, 1997. Thirty-Second IAS Annual Meeting, IAS '97., Conference Record of the 1997 IEEE*, 1997, vol. 1, pp. 775-780 vol.1.
[18] I. M. Alsofyani and N. R. N. Idris, "Simple Flux Regulation for Improving State Estimation at Very Low and Zero Speed of a Speed Sensorless Direct Torque Control of an Induction Motor," *IEEE Transactions on Power Electronics*, vol. 31, no. 4, pp. 3027-3035, 2016.
[19] I. M. Alsofyani, N. R. N. Idris, Y. A. Alamri, S. A. Anbaran, A. Wangsupphaphol, and W. Y. Low, "Improved EKF-based direct torque control at the start-up using constant switching frequency," in *Energy Conversion (CENCON), 2014 IEEE Conference on*, 2014, pp. 237-242.
[20] A. B. Jidin, N. R. B. N. Idris, A. B. M. Yatim, T. Sutikno, and M. E. Elbuluk, "Extending Switching Frequency for Torque Ripple Reduction Utilizing a Constant Frequency Torque Controller in DTC of Induction Motors," *Journal of Power Electronics*, vol. 11, no. 2, pp. 148-154, 2011.
[21] N. R. N. Idris and A. H. M. Yatim, "Direct torque control of induction machines with constant switching frequency and reduced torque ripple," *IEEE Trans. Ind. Electronics*, vol. 51, no. 4, pp. 758-767, 2004.
[22] Y. R. Kim, S. K. Sul, and M. H. Park, "Speed sensorless vector control of induction motor using extended Kalman filter," *IEEE Trans. Ind. App.*, vol. 30, no. 5, pp. 1225-1233, 1994.
[23] W.S.H. Wong and D. Holliday, "Minimisation of flux droop in direct torquecontrolled induction motor drives," 2004.
[24] I. M. Alsofyani, N. R. N. Idris, and Y. A. Alamri, "An improved flux regulation using a controlled hysteresis toque band for DTC of induction machines," in *2015 IEEE Conference on Energy Conversion (CENCON)*, 2015, pp. 368-372.
[25] Y. Li, J. Shao, and B. Si, "Direct torque control of induction motor for low speed drives considering discrete effects of control and dead-time of inverter," in *Industry Applications Conference, 1997. Thirty-Second IAS Annual Meeting, IAS '97., Conference Record of the 1997 IEEE*, 1997, vol. 1, pp. 781-788 vol.1.

Ibrahim Mohd Alsofyani (M'16) received the B.Eng. degree in electronics engineering from Multimedia University, Melaka, Malaysia, in 2008, and the M.Eng. degree in electrical- mechatronics and automatic control and the Ph.D. degree both from the Universiti Teknologi Malaysia, Johor Bahru, Malaysia, in 2011 and 2014, respectively. From 2014 to 2016, he was a research associate and then postdoctoral fellow at the UTM-PROTON Future Drive Laboratory, Universiti Teknologi Malaysia. From 2016 to 2017, he worked as a lecturer in the Faculty of Engineering, Lincoln University College, Selangor, Malaysia. Currently, he is a research professor at the power electronics lab, School of Electrical and Computer Engineering, Ajou University, Suwon, Korea. His current research interests include electric machine drives, renewable power generations and electric vehicle applications.

Nik Rumzi Nik Idris (M'97, SM'03) received the B.Eng. degree in Electrical Engineering from the University of Wollongong, Australia, the M.Sc. degree in power electronics from Bradford University, West Yorkshire, U.K., and the Ph.D. degree from Universiti Teknologi Malaysia (UTM) in 1989, 1993, and 2000, respectively. He is currently an Associate Professor at the Universiti Teknologi Malaysia, and the head of Power Electronics and Drives Research Group. He is also the past chair for the Power Electronics Society, Malaysia Chapter. His research interests include control of ac drive systems and DSP applications in power electronic systems.

Kyo-Beum Lee (S'02–M'04–SM'10) received his B.S. and M.S. degrees in Electrical and Electronic Engineering from Ajou University, Suwon, Korea, in 1997 and 1999, respectively. He received his Ph.D. degree in Electrical Engineering from Korea University, Seoul, Korea, in 2003. From 2003 to 2006, he was with the Institute of Energy Technology, Aalborg University, Aalborg, Denmark. From 2006 to 2007, he was with the Division of Electronics and Information Engineering, Chonbuk National University, Jeonju, Korea. In 2007, he joined the School of Electrical and Computer Engineering, Ajou University. His current research interests include electric machine drives, renewable power generations and electric vehicle applications. Prof. Lee is an Associated Editor of the IEEE Transactions on Power Electronics, the Journal of Power Electronics, and the Journal of Electrical Engineering and Technology.